Electronically stimulated dissociation of NO_2 on Pt(111)

A. R. Burns, D. R. Jennison, and E. B. Stechel

Sandia National Laboratories, Division 1151, Albuquerque, New Mexico 87185

(Received 1 May 1989)

The electronically stimulated dissociation of NO_2 on Pt(111) by 5–800-eV electrons has been studied through state-selective, time-of-flight detection of the NO product above the surface. The NO leaves as a direct dissociation product, whereas the O atom remains on the surface. We find a 10–15-eV dissociation threshold, which is much more energetic than the 3.1-eV gas-phase value. Because of rapid decay via resonant tunneling from substrate levels, the shallower adsorbate valence excitations have lifetimes that are too short to produce observable dissociation. The threshold corresponds to ionization of $3b_2$ and double ionization of $1a_2$ levels. Holes in these levels cannot be resonantly filled by substrate electrons and have the longest lifetimes relative to Auger decay. Screening of the hole(s) by the metal proceeds via rehybridization between the substrate levels and the $6a_1$ orbital of the molecule. The screening charge not only determines the lifetime, but is expected to change the excited-state ONO bond angle and NO bond length. In the gas phase this results in considerable internal excitation of the NO product. On the metal surface, however, vibrational excitation above $v=2$ is not observed: The relative populations for $v=0,1,2$ are (1.0):(0.96):(0.52). The average rotational energy (800 K for each vibrational level) is only 50% warmer than the zero-point energy of the ground-state bending motion of the adsorbate. Thus the screening charge must be less than unity. The observation of shifts to higher translational energy for higher rotational and vibrational states indicates the presence of different charge-transfer screening densities for the $3b_2^{-1}$ and $1a_2^{-2}$ excitations.

I. INTRODUCTION

In this paper we are concerned with molecular dissociation on metal surfaces initiated by the electronic excitation of the adsorbed molecules. Electronic excitation of adsorbed species is well known to cause photochemical reactions, as well as photon- and electron-stimulated desorption.[1] Recently, there has been interest in examining the effects of the metal substrate on the yields and dynamics of photodissociation processes which have been well characterized in the gas phase.[1-4] It is clear that the metal surface will influence the course of the stimulated process by greatly reducing the lifetime of the electronic excitations by screening, charge transfer,[2] or other nonradiative couplings.[5] Not only will the yield of stimulated surface processes be determined by lifetimes, but also the entire dynamics of the process will be influenced by the bonding geometry and electronic structure of those excited states that have sufficient lifetimes ($> 10^{-14}$ sec) to allow nuclear motion to occur.[6]

A complete picture of stimulated dissociation and/or desorption requires knowledge of (1) the nature and localization of the "responsible" electronic excitation in the adsorbed species, (2) the atom motion on the excited-state potential energy surface, and (3) the chemical identity and translational and internal energies of the products. In previous work[1,6,7] we have shown that electron-stimulated desorption (ESD) of neutral NO from Pt(111) was dominated by one channel due to the relatively long lifetime of a 5σ hole in the adsorbate. Lifetime calculations ruled out other single-hole excitations such as that involving the 1π orbital, which is nearly isoenergetic with

the 5σ hole for NO on Pt.[8] The vibrational distribution of the desorbed NO over $v=0,1,2,3$ was consistent with the partial presence of a 2π screening electron from the metal caused by rehybridization of the bonding 2π-metal orbital in the excited state.[9] Two-dimensional quantum-dynamical calculations for atom motion on this excited-state potential energy surface, followed by lifetime decay to the ground state, reproduced translational and rotational energy distributions of desorbed NO.[9]

Here we use a similar approach to characterize the electronically stimulated dissociation of NO_2 on Pt(111), i.e., we seek information on the electronic structure of the long-lived excitation states and examine the dissociation dynamics. Quantum-specific information on the threshold, yield, translational, and internal energies are presented for the gas-phase NO product of stimulated NO_2 dissociation. A direct comparison of this work with previous gas-phase uv photodissociation studies provides unique insight into the strong influence of the substrate on electronically stimulated surface processes. We are able to analyze the effects of metal screening on the dissociative excitation lifetimes and dynamics. We find that the extensive vibrational and rotational excitation observed in gas-phase photodissociation is absent for adsorbate dissociation. We also find that most of the simple one-electron excitations responsible for gas-phase dissociation are too short lived to be effective on the surface.

Since the gas-phase work is essential for our analysis, we have summarized the current literature in Sec. II. In Secs. III and IV we present the experimental details and results, respectively. The discussion in Sec. V focuses on experimental results and the electronic structure analysis,

including peak assignments for the ultraviolet photoelectron spectrum (UPS) of NO_2 adsorbed on Pt(111).[10]

The adsorption geometry and thermal decomposition of NO_2 on Pt(111) have been carefully analyzed by Bartram, Windham, and Koel.[11] The authors find that molecular adsorption occurs at temperatures below 170 K in a bridge-bonded nitrito complex where the molecule is bonded side-on, coordinating the nitrogen atom and one oxygen atom to the metal, while the other oxygen atom points away from the surface. Although it has not been confirmed, their analysis of the stretching frequencies of the adsorbate indicates that the ONO bond angle may be reduced to as much as 115° from the gas-phase 134°; thus the noncoordinated NO bond would be approximately 25° from the surface normal.

II. SUMMARY OF GAS-PHASE NO_2 PHOTODISSOCIATION RESULTS

Gas-phase uv photodissociation of NO_2 into NO and O occurs with essentially unit quantum yield[12] above the 3.1-eV (25 000 cm^{-1}) threshold, and thus has been the topic of extensive investigation by many groups. The importance of understanding the molecular dynamics of NO_2 dissociation was made clear by the photofragment work of Busch and Wilson.[13] With an excitation energy 3700 cm^{-1} (0.46 eV) above the dissociation threshold, they found that the total translational energy of both fragments exceeded 0.4 eV (3100 cm^{-1}) for the ground vibrational state $(v=0)$. However, they noticed a significant peak at 0.2 eV, which they attributed to $v=1$ NO. It was found that the NO fragments acquired about one-third of the translational energy: 0.14 eV for $v=0$ and 0.07 eV for $v=1$. A similar value for the NO($v=0$) fragment translational energy following 360-nm (0.33 eV excess) photodissociation has been reported.[14]

The partitioning of excess energy into translational and internal degrees of freedom was analyzed in more detail by Zacharias et al.,[15] who used state-selective detection to examine the actual rotational and vibrational distributions of the NO fragment. Although the latter experiments involved a larger excess energy (0.56 eV), they found that a much larger percentage was found in the internal modes (only 0.18 eV estimated to be in translation). The internal energy distributions were also completely nonstatistical, with an inverted vibrational distribution (over $v=0,1,2$) and rotational populations observed at the thermodynamic limit. The rotational population had two distinct regions: at low J the average energy was 65 K, whereas at high J the average energy was 1600 K.

The gas-phase data of Zacharias et al. made it evident that at this excitation energy NO_2 must undergo large changes in geometry relative to the $^2A_1$ ground state. Indeed, the predissociative $\tilde{A}\,^2B_2$ state at 16 850 cm^{-1} (2.089 eV) above the $^2A_1$ state does have a smaller ONO bond angle, $\alpha=111°$ (compared to the ground state, $\alpha=134°$), and longer NO bonds ($r_0=1.23$ Å compared to $r_0=1.19$ and 1.15 Å for ground-state NO_2 and NO, respectively).[16,17] The geometry of the $^2B_2$ state is associated with the promotion of a $4b_2$ electron to the normally

singly occupied, antibonding $6a_1$ orbital (using Herzberg's notation[16]). By increasing the excess photon energy to 15 480 cm^{-1} (1.92 eV), Slanger et al.[18] were able to show that the dissociation dynamics remained essentially the same; only now the vibrational distribution peaked at $v=7$ (with $v=8$ the new thermodynamic limit). At this photon wavelength (248.5 nm), the $\tilde{B}\,^2B_2$ state is also accessible. The bonding geometry for the $\tilde{B}\,^2B_2$ state has been determined[19] to have $\alpha=121°$ and $r_0=1.31$ Å; thus the mechanism for vibrational excitation is further enhanced. In similar experiments, Grant et al.[20] found that as soon as the 243-nm (41 000 cm^{-1}) threshold for production of excited $O(^1D)$ was reached, vibrational excitation was reduced. Although no $O(^1D)$ was detected in these experiments, the presence of $v=0$ NO was attributed to $O(^1D)$ production. With this in mind, Grant et al.[21] estimated the relative yield of excited $O(^1D)$ to ground-state $O(^3P)$ at 1:4.

More recently, Slanger et al.[22] raised the excitation energy to 157.6 nm (63 450 cm^{-1}), well past the 58 000-cm^{-1} origin of the linear $^2\Sigma_2^+$ Rydberg state [$\alpha=180°$ and $r_0=1.1$ Å (Ref. 16)]. Despite an excess energy of 38 600 cm^{-1} (4.79 eV), the dissociation dynamics remain the same: extensive vibrational excitation ($v=21$ observed, $v=25$ being the limit) and very high rotational excitation. No excited $O(^1D)$ was detected. The absence of $O(^1D)$ placed the experimental upper limit of $O(^1D)$ production at $<10\%$ of $O(^3P)$. The natures of the excited states above the $\tilde{B}\,^2B_2$ state remain ambiguous, although vibrational progressions in the 135–165-nm absorption spectrum indicate a linear molecule with short bond lengths (1.13 Å).[23]

In summary, the dominant products of uv photodissociation up to 157.6 nm (7.6 eV) are ground-state $O(^3P)$ and ground-state NO that has vibrational excitations up to the limit of excess photon energy and substantial rotational excitation. Unfortunately, the data above 330 nm excitation do not include translational energies. The internal excitations at the lower photodissociation energies are due to double occupation of the antibonding $6a_1$ orbital in the $\tilde{A}\,^2B_2$ and $\tilde{B}\,^2B_2$ states.

III. EXPERIMENT

All the experiments discussed below were conducted in an ion-pumped vacuum chamber with a base pressure below 5×10^{-11} Torr. The chamber is equipped with a single-pass cylindrical mirror analyzer for Auger-electron spectroscopy (AES), a quadrupole mass spectrometer (QMS), a pulsed electron gun, and a multichannel-plate (MCP) time-of-flight (TOF) apparatus for the detection of ions produced by the laser resonance ionization of desorbed neutral molecules. Details concerning the TOF geometry and its computer control have been published elsewhere.[1,6,24] The polished Pt(111) crystal[25] can be resistively heated to 1200 K and cooled to less than 100 K. A type-K (Chromel-Alumel) thermocouple is in contact with the side of the crystal for temperature measurements.

The Pt crystal was initially cleaned by ion bombardment, followed by annealing at 1200 K. Cleanliness was

confirmed by the absence of $C(KLL)$, $Ca(LMM)$, $O(KLL)$, etc., in the AES. After initial cleaning, the crystal was recleaned by resistive heating to 1200 K. However, after many cycles of NO₂ dosing followed by thermal desorption and decomposition into NO and O, it was found by AES that a substrate oxide developed.[26] This was then removed by ion bombardment, followed by annealing as before.

The NO₂ was purchased from Alphagaz (99.995% purity) and handled in a stainless-steel gas manifold equipped with a glass cold finger. The baked gas manifold had been originally passivated by acid cleaning, but had to be further passivated by many hours of exposure to NO₂ gas. Before the crystal was dosed, the NO₂ in the manifold was subjected to at least three freeze-pump-thaw cycles in the cold finger, where the pure-white N₂O₄ crystals could be seen. The passivated dosing port consists of a small tube in front of the crystal which allows for high dose rates without letting the chamber pressure exceed 2×10^{-10} Torr. This was particularly important in the acquisition of $v=0$ rotational spectra of the NO dissociation product because the chamber had to be pumped down for several minutes to below 6×10^{-11} Torr before the residual NO background due to NO₂ decomposition on the chamber walls was negligible.

Adsorption of NO₂ on the clean Pt(111) crystal was confirmed by examining the thermal-desorption spectra (TDS) as shown in Fig. 1. The large N₂O₄ ice peak at 140 K, and the thermal decomposition of NO₂ resulting in the NO peak at 300 K and the large O₂ peak at 700 K, agree qualitatively with known spectra[11] from a crystal dosed at 100 K. Quantitative differences arise because the QMS mass filter is not in the line of sight of the crystal; thus the N₂O₄ ice layer, desorbed as NO₂, is detected as NO due to dissociation on the chamber walls. Similarly, the observation of NO desorption above 400 K is due to desorption from the crystal holder and not due to the

presence of defect sites.[27] The latter is discounted by the complete lack of O₂ and N₂ desorption[27] in the TDS of NO from the clean surface. The QMS filter is programmed to switch from mass 30 (NO) to mass 32 (O₂), so that both signals are collected in each TDS run. *In all the work described below, the crystal temperature was kept at 150 K during the NO₂ dosing, so that the NO₂ was adsorbed molecularly[11] and no N₂O₄ ice layer was allowed to form.* Following the dose, the crystal was rotated away from the dosing port and allowed to rapidly cool to below 100 K. All the data were collected at this low temperature. After the data acquisition, the TDS was examined to confirm the absence of the ice layer and to make sure there was no additional NO peak at 200 K, which indicates contamination of the NO₂ with NO.[27] Except where noted, the NO₂ coverage was at saturation,[11] 0.5 monolayer (ML), or 7.5×10^{14} molecules/cm², for all the experiments. Lower coverages were determined by integration of the O₂ thermal desorption peak relative to the saturation value.

The electron gun is situated at an angle of 45° to the sample surface and produces $0.3-1.2$-μs pulses, with a peak intensity of 6×10^{16} electrons/cm²s. All the experiments are conducted in the TOF mode, whereby the pulse of neutral particles produced by the electron beam traverse a 0.5-cm distance before they are resonantly ionized at a specified delay time by the 4-ns laser pulse focused into a 0.2-mm-thick, 0.5-cm-wide ribbon. The laser-beam area of > 0.5 cm² is sufficient to angle-integrate most of the neutral particles. The focus and energy (E_{HV}) of the electron beam are computer controlled to ensure a constant spot size (0.02 cm²) on the sample (0.78 cm²) at all times (except below 20 eV, as discussed below).

The TOF translational-energy distributions are obtained by computer-programmed stepping in delay time corresponding to linear steps in desorbate translational energy. Although the data are automatically scaled in energy and have been corrected for the velocity dependence of the particle density in the laser beam, there is still an intrinsic error due to the velocity spread ($\Delta V/V$) arising from the 300-ns width of the electron-beam pulse. The spread is $\Delta V/V = 0.3$ at 0.05 eV, but increases to $\Delta V/V = 0.12$ at 0.6 eV. The larger spreads at shorter delay times naturally increase signal strength. In order to properly correct for this, however, the velocity distribution must be known beforehand. Such is the case when the data are compared with theory.[1] For the present, the TOF distributions are best suited for observing relative changes (e.g., due to changes in surface chemistry).

Threshold measurements are obtained by a computer-controlled sweep of the electron-beam energy E_{HV} and focus for a fixed E_{trans} (i.e., delay time). For all threshold data and rotational spectra (see below), the width of the electron beam is increased to at least 1.0 μs to span the peak of the translational-energy distribution. At $E_{HV} < 20$ eV, the beam current remains constant, but it becomes steadily more difficult to keep the beam-spot size on the surface from increasing. To make sure that the threshold data are strictly for those molecules adsorbed on the Pt(111) crystal and do not include contributions
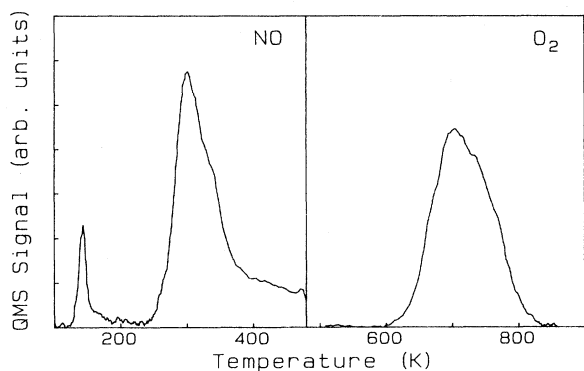

FIG. 1. Thermal-desorption spectra of NO₂ (> 3 ML) initially adsorbed on Pt(111) at 100 K. The heating rate was approximately 4 K/s. The quadrupole mass spectrometer (QMS) was not in the line of sight of the crystal, so that NO₂ was difficult to observe directly, and the relative peak heights may differ from other studies. The small NO peak at 140 K is attributed to N₂O₄ ice desorbing as NO₂ and subsequently dissociating on the walls and in the QMS ionizer.

from off the crystal, it is necessary to subtract the background signal. The background signal is easily acquired by repeating the scan after the NO_2 has been thermally desorbed. This technique is particularly important in the case of NO_2, since it readily sticks everywhere.

The NO rotational energy distribution for a given vibrational level v'' is obtained by scanning the laser for a fixed E_{HV} and E_{trans} (Refs. 1 and 6) through the well-known $A\,^2\Sigma^+(v') \leftarrow X\,^2\Pi_{1/2,3/2}(v'')$ resonance-enhanced $(1+1)$ ionization.[28,29] The tunable uv is generated by mixing the frequency-doubled output of a Nd^+:YAG-pumped dye laser with the 1064-nm fundamental of the Nd^+:YAG laser (YAG denotes yttrium aluminum garnet). The output of the dye laser was calibrated with a Ce-Ne hollow cathode lamp. The beam intensity is approximately 40 mJ/cm^2 in the ribbon-shaped ionization region. Saturation and alignment effects[29] were calibrated by comparison of calculated intensities[30] and the room-temperature $v=0$ NO gas-phase spectrum acquired for NO bled into the vacuum chamber ("bulb" spectrum in Table I) and taken under the same focusing and intensity conditions as above. For each spectrum, the rotational line positions[31,32] were calculated and used to determine the spectral resolution and the rotational populations.

In all the experiments the integrated laser-beam energy was monitored on a shot-to-shot basis with a pyroelectric detector and stored in the computer. Prior to the acquisition of threshold and TOF data, the computer collected 500 laser pulses for a least-squares fit to determine the energy dependence of the signal. This was then used by the same program to normalize the signal for each shot; data for laser energies falling outside the 500-point array were discarded. This technique is not used for the rotational spectra since each rotational band has a different energy dependence.[29] In this case, the 500-point array of laser energies is used to determine the mean pulse energy. All the rotational spectra were then collected with data points obtained with laser energies within 15% of this mean.

IV. RESULTS

A. NO escape, O retention

We conclude from the translational energy distributions and other dynamical effects discussed below that the NO product of the electron-beam-induced NO_2 dissociation directly leaves the surface. However, NO detection still leaves some critical questions: (1) Does the O-atom product leave the surface? (2) Is the NO signal due to the ESD of NO_2, which is subsequently photolyzed by the laser? The answer to both questions is "no." Evidence for these conclusions can be found from the following surface and gas-phase experiments.

The first experiment examines the relative changes in the N(KLL) and O(KLL) signals in the Auger spectra (AES) of the NO_2-covered Pt surface (0.5 ML) before and after a 35-min exposure to a continuous 500-eV electron beam (0.18 μA). The electron beam is provided by the Auger gun itself; thus the $\sim$0.004-cm^2 (estimated) beam

spot stays aligned with the probe beam. The AES are obtained with a probe energy of 2000 eV and are computer averages of ten spectra that are rapidly scanned (25 s) from 200 to 550 eV. One can see from Fig. 2 that after subtraction of the Pt signal at 390 eV (where the peak-to-peak ratio $I_{Pt(390)}/I_{Pt(237)}=0.17$, as observed by Gland[33]), the peak-to-peak N(KLL) signal is reduced by 55%, whereas the peak-to-peak O(KLL) signal is reduced by 25%. If NO_2 is desorbed directly, or if O atoms leave the surface along with the NO, then the percentage of N and O lost should be identical. The 2:1 ratio in losses therefore must be attributed to the escape of NO and the retention of O. Since heating of the 100-K substrate is precluded by the low current density, this effect must be due to electron-induced dissociation.

The retention of O on the Pt surface is confirmed by the complete lack of signal at 225.6 nm (pulse energies >100 mJ/cm^2) for the $(2+1)$ resonance ionization of ground-state $O(^3P)$. Using the cross sections measured by Bamford et al.[34] for the two-photon $3p\,^3P \leftarrow 2p\,^3P$ resonant step and the one-photon ionization step, one can estimate that at a laser intensity of 100 mJ/cm^2 at least 0.1% of the oxygen atoms entering the laser beam should be ionized. Since our detection limit is $\sim 3 \times 10^3$ $ions/cm^3$ in the laser-ionization volume, the upper limit of the $O(^3P)$ density is $\sim 3 \times 10^6$ $atoms/cm^3$. As will be discussed below, the density of $NO(v=0)$ in the ion laser beam is $\sim 4 \times 10^6$ $molecules/cm^3$. Thus $O(^3P)$ would be detected if it were leaving the surface with a comparable flux.

The absence of $O(^3P)$ signal also confirms the AES result that no intact NO_2 molecules are desorbed and subsequently photolyzed in the laser beam (see Sec. II). Even so, two more tests were employed to make sure no NO_2 is being desorbed. The distinctive $(2+2)$ resonance ionization of NO_2 at 511 nm (Ref. 35) was used to look directly for desorbed NO_2. No signal was observed for laser intensities exceeding 500 mJ/cm^2. Finally, no signal for the NO $v=5$ level at 284.9 nm was observed. As was discussed in Sec. II, a large population of $v=5$ NO is pro-

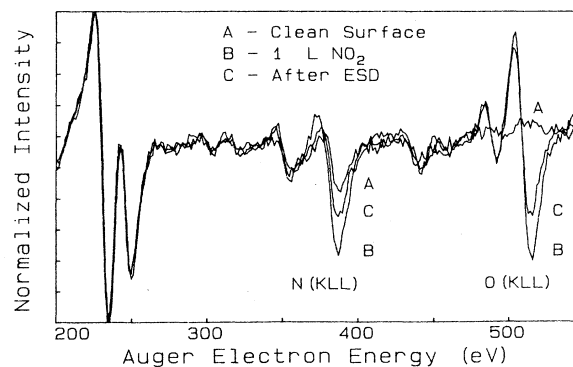FIG. 2. Auger-electron spectra (AES) of A, a clean Pt(111) surface prior to NO_2 adsorption; B, 0.5 monolayer (ML) of NO_2; C, 0.5 ML NO_2 following ESD by 500-eV electrons (see text for details). The spectra are normalized with respect to the Pt(111) signal at 237 eV.

duced by photodissociated NO$_2$ at 284.9 nm.[18]

The yield of the NO($v=0$) dissociation product at 350 eV excitation is estimated by comparing the signal strength measured at the peak of the translational energy distribution (0.11–0.16 eV; see next section) and saturation coverage (7.5×10^{14} molecules/cm^2) with the signal obtained under identical resonance-ionization conditions for gas-phase NO bled into the chamber. The NO density in the laser beam is actually calculated in a more precise fashion in that the individually resolved $v=0$ rotational lines are summed for both the "bulb" NO and the desorbed NO. Since the electron-beam flux is 6.0×10^{16} electrons/cm^2 s (0.016-cm^2 beam area) during the electron-beam pulse, and the observed density of 4×10^6 (NO molecules)/cm^3 in the 0.5-cm^2 laser beam have a velocity of $\sim1\times10^4$ cm/s, the cross section for 350-eV electron-stimulated dissociation is estimated to be 1.0×10^{-18} cm^2. The total dissociation cross section is, of course, higher because it must include vibrationally excited molecules (see Table I) and those molecules not in the 0.11–0.16-eV translational-energy window. Taking these factors into account, the total yield of $\sim5\times10^{-18}$ cm^2 is comparable to ESD cross sections for neutral molecules,[36,37] but considerably less than the cross section for gas-phase electron-impact dissociation[38] (3×10^{-17} cm^2) and uv photodissociation. The NO yield from NO$_2$/Pt varies smoothly with electron beam energy as will be shown in Sec. IV D.

B. NO translational-energy distributions

Translational energy (E_{trans}) distributions for the NO($v=0$) product from the dissociation of NO$_2$ on Pt(111) by 350-eV electrons are shown in Figs. 3–6. In Fig. 3 a comparison is made between the E_{trans} of NO($v=0$) resulting from NO$_2$ dissociation and that from the ESD of NO adsorbed on Pt(111). It is clear that the dissociation product exhibits a higher peak E_{trans} and a
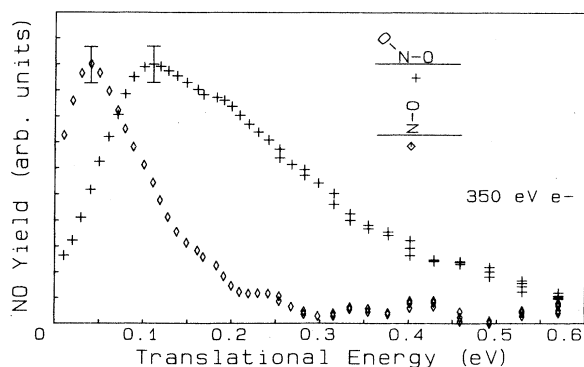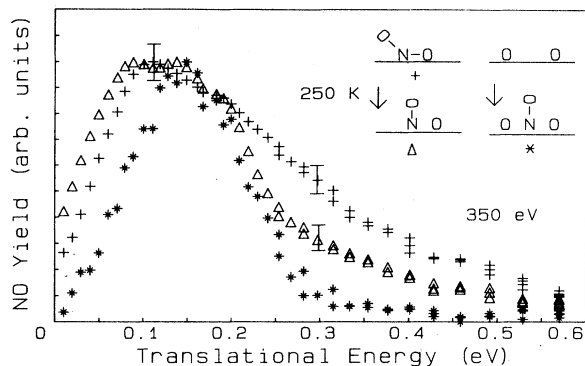

FIG. 4. Comparison of the TOF E_{trans} distribution for the NO product of NO$_2$ (0.5 ML) dissociation on Pt(111) with the distribution of NO ESD coadsorbed with 0.75 ML of O and the distribution of NO ESD from thermally dissociated NO$_2$ (0.5 ML) on Pt(111). The data were acquired at the P_{11} bandhead ($J=6.5$–11.5) for the $v=0$ level. They are normalized with respect to the peak (not to the actual yield) for purposes of comparison.

much broader high-energy tail than that seen in the NO ESD data.

A more interesting E_{trans} comparison is between the dissociation product and the ESD and NO coadsorbed with O. Differences in the respective E_{trans} (and internal) energies reflect direct desorptive dissociation, rather than an uncorrelated two-step process involving dissociation followed by ESD of the NO product. An uncorrelated two-step process would mean that all dynamical information concerning the dissociation is lost and the data would only reflect the ESD of NO coadsorbed with O. Two coadsorption experiments were conducted. In the first, 0.75 ML of O atoms on Pt(111) was produced by exposing the Pt surface to >30 L (1 L$=1$ langmuir$\equiv10^{-6}$
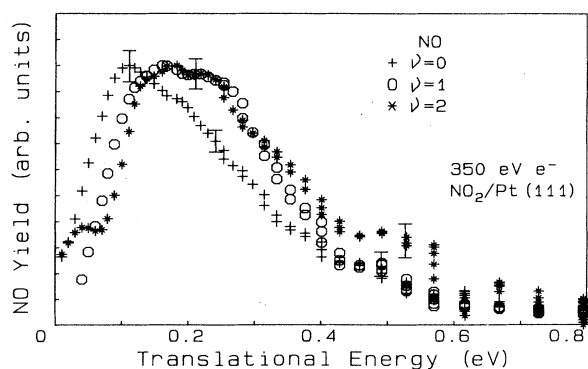

FIG. 3. TOF translational energy (E_{trans}) distribution for the NO($v=0$) product of NO$_2$ (0.5 ML) dissociation on Pt(111). Also shown for comparison is the distribution for ESD of NO($v=0$) on Pt(111). The data were acquired at the P_{11} bandhead ($J=6.5$–11.5) and normalized with respect to the peak (not to the actual yield) for the purpose of comparison.

FIG. 5. Comparison of the TOF E_{trans} distributions for the three observed vibrational levels ($v=0,1,2$) of the NO product of NO$_2$ (0.5 ML) dissociation on Pt(111). The data were acquired at the P_{11} bandhead ($J=6.5$–11.5) and normalized with respect to the peak (not to the actual yield) for purposes of comparison.
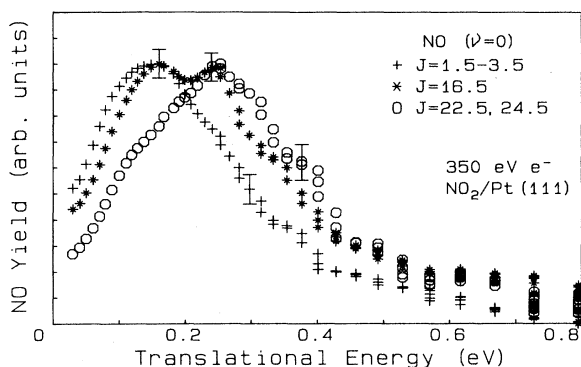
FIG. 6. Comparison of the TOF E_{trans} distributions as a function of rotational energy for the $v=0$ NO product of NO_2 (0.5 ML) dissociation on Pt(111). The low-J distribution was obtained at the $P_{21}Q_{11}$ bandhead ($J = 1.5-3.5$). The intermediate-J distribution was obtained at the $R_{11}Q_{21}$ ($J = 16.5$) line. The high-J distribution was obtained at the $P_{21}Q_{11}$ ($J = 24.5$) line, which overlaps the weaker R_{22} ($J = 22.5$) line. All three distributions were normalized with respect to the peak (not to the actual yield) for purposes of comparison.

Torr s) of NO_2 while keeping the crystal temperature at 400 K.[39] The O-covered crystal was then exposed at 150 K to <1 L of NO. One can see in Fig. 4 that the E_{trans} distribution for the ESD of NO coadsorbed with O is clearly narrower than that obtained from dissociation. A significant shift to higher energy is seen in the entire NO ESD E_{trans} distribution in going from the clean surface to 0.75 ML of coadsorbed O. It should be pointed out that bond formation of the NO with coadsorbed O to form NO_2 on the surface has been ruled out by the absence of the correct vibrational frequencies and the absence of NO_2 thermal desorption.[40]

The second method of producing coadsorbed NO and O (also seen in Fig. 4) is by heating a NO_2 layer to 250 K and allowing it to cool back to 100 K. In this case there are still remnants of a high-energy tail, but also a slight shift in the peak to lower energies. The thermally dissociated NO_2 data thus seem to have contributions from several species: NO isolated from O, NO with one O-atom neighbor, NO with two neighbor O atoms, and some undissociated NO_2. A detailed study of the O-atom coadsorption effects on the ESD of NO is underway, but for the present purpose it is clear that the translational energies of the NO_2-covered surface are distinct from the NO, O-covered surface and thus reflect the dissociation dynamics directly.

In Fig. 5 we exploit the state selectivity of the resonance-ionization technique and examine the E_{trans} distributions as a function of vibrational energy in the NO dissociation product. One can see that there is a slight shift to higher E_{trans} for the $v=1,2$ populations relative to that observed for $v=0$. Much larger shifts in E_{trans} with increasing vibrational energy were observed previously in the ESD of NO.[6] In the latter work the shifts were due to the presence of two distinct desorption

channels, the low E_{trans} peak involving a one-hole excitation and the higher E_{trans} peak involving two-hole or higher excitations.

When E_{trans} is examined as a function of NO($v=0$) rotational energy, one can see in Fig. 6 that there is a distinct shift to higher E_{trans} with increasing rotational energy of the dissociation product. The double-peaked distribution in Fig. 6 for an intermediate rotational level suggests that the shift is indeed due to the presence of two dissociation channels. It should be pointed out that no shift in E_{trans} with increasing rotational energy is observed in the ESD of NO.[7]

No changes in the E_{trans} data for NO($v=0,1$) were observed as a function of NO_2 coverage. Thus there appear to be no nearest-neighbor interactions that may alter the dissociation dynamics. Unfortunately, the low signal-to-noise ratio for the rotationally hot species gets worse at low NO_2 coverages, so that an investigation determining the effect of nearest-neighbor interactions for these molecules is difficult.

C. Coverage dependence

A very weak increase in the specific yield of NO is observed for decreasing NO_2 coverage on the Pt(111) crystal. The data shown in Fig. 7 are obtained by integrating the entire NO($v=1$) TOF distribution at a specific coverage. The TOF integrated data are then normalized to the integrated area under the O_2 thermal-desorption peak. The coverage dependence is similar to that observed for the single-hole excitation ESD of NO for $\Theta > 0.15$ ML; the latter has a specific yield which increases rapidly at $\Theta < 0.15$ ML due to the increased probability for localization of the electronic excitation.[24] Thus the slight dependence seen here may be due to more effective localization of the electron excitation, which is necessary before stimulated dissociation can occur.
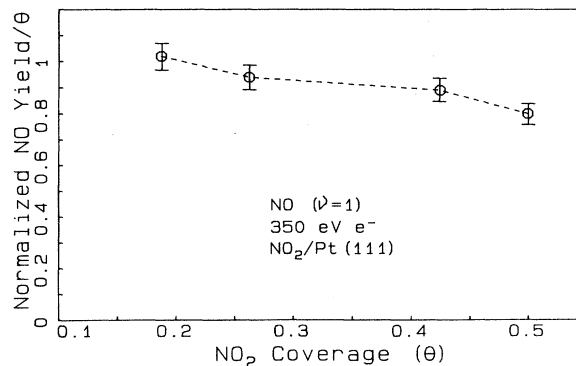

FIG. 7. Dependence on the NO($v=1$) product yield on the NO_2 coverage. The specific yield [(NO signal)/Θ] is obtained by normalizing the integrated TOF distribution with the O_2 peak obtained by subsequent thermal desorption. Saturation coverage is $\Theta = 0.5$ (Ref. 11).

D. Threshold for electron-stimulated dissociation

The minimum electron energy required to excite the adsorbed NO_2 to a sufficiently "long-lived" dissociative state is manifested in the threshold for NO production. The observed thresholds for $\nu=0$ and 1 NO are shown in Fig. 8, where the delay time of the laser pulse is set to detect the peak of the translational energies. Here we assume that the final states of the primary electron and the excited NO_2 electron are at the Fermi level of the substrate. Thus the excitation energy shown in Fig. 8 is given by $E_{HV}+\phi_C$, where E_{HV} is the beam voltage and ϕ_C is the work function of the electron-gun cathode (4.1 eV). The data tend to be very noisy due to the reduced excitation cross section at these low electron energies and the fact that subtraction of the background (crystal holder) is necessary (Sec. III). Negative biasing of the crystal can eliminate the need for background subtraction, but then spurious field effects are observed above the threshold. In order to signal-average as long as possible, the $\nu=1$ scan goes only as far as 46 eV; the $NO(\nu=2)$ threshold data were too noisy to be conclusive. In numerous scans both the $NO(\nu=0)$ and $NO(\nu=1)$ threshold are in the range 10–15 eV; thus there are no obvious differences in the $\nu=0$ and 1 excitation channels that can account for the observed shifts in the E_{trans} data with vibrational energy. The same can be said for the shifts in E_{trans} with rotational energy since thresholds for both the high and low rotational states discussed above were also roughly in the same energy range of 10–15 eV. Thus the two channels that would account for the E_{trans} shifts with increasing internal energy appear to have approximately the

FIG. 9. Yield vs excitation energy for the $NO(\nu=1)$ product of NO_2 (0.5 ML) dissociation on Pt(111). The curve for $NO(\nu=0)$ is identical, within experimental error, for the equal $\nu=0$ and 1 populations (Table I). The yield scale (including contributions for all E_{trans}) at the left is thus valid for each level. It is calibrated by measurements of the $NO(\nu=0)$ density in the laser beam resulting from 350-eV excitation (Sec. IV A). The dashed lines are drawn through the N(1s) and O(1s) core-level edges.

same threshold energy.

The threshold data are far from precise, but they do indicate that the dissociation is due to a one-hole and/or a two-hole valence excitation well above the 3.1-eV gas-phase dissociation threshold (Sec. II). Although cascading from higher-lying "entry channel" states to the 10–15-eV primary valence excitation(s) always occurs, there appears to be no structure in the yield above threshold that indicates that specific high-energy entry channels are dominating. Similarly, it can be seen from Fig. 9 that there is no effect on the dissociation yield at the N(1s) and O(1s) core-excitation thresholds. Unlike ion desorption resulting from molecular dissociation processes on surfaces,[3,41,42] core-level excitation does not appear to directly contribute in an observable manner to the neutral product formation. Thus we conclude that the dissociation of NO_2 into neutral NO and O is dominated by a valence-level excitation(s).

E. Internal energies of NO product

Like the threshold data, the rotational energy distributions for the $\nu=0,1,2$ levels are obtained at a fixed delay time corresponding to the peak of E_{trans}. The rotational energy distribution for $NO(\nu=0)$ is shown in Fig. 10. However, as seen in Fig. 6, the peak translational energy shifts with increasing rotational energy. Verification of the shift in E_{trans} at high J is shown in Fig. 11, where the rotational spectra at two delay times are compared. Since there does appear to be two dissociation channels, the following discussion corresponds only to the channel with the lower E_{trans} (0.11–0.16 eV for $\nu=0$). Despite the possible loss of signal for high rotational levels, the average rotational energy is still 862 ± 30 K for $\nu=0$. (Clearly, the higher E_{trans} channel has a much more energetic distribution heavily weighted with high-J com-
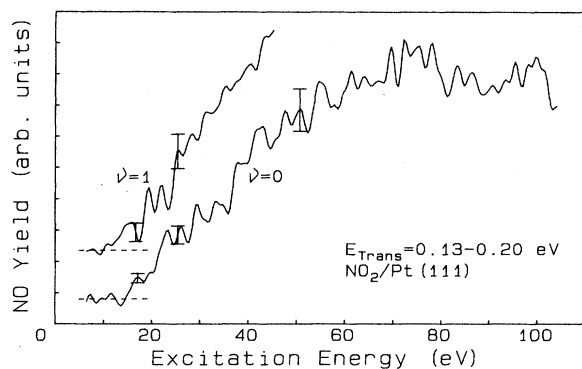
FIG. 8. Thresholds for the $\nu=0,1$ levels of the NO product of NO_2 (0.5 ML) dissociation on Pt(111). The excitation energy is given by $E_{HV}+\phi_C$, where E_{HV} is the electron acceleration voltage with respect to the sample (and electron gun) ground, and ϕ_C is the work function of the cathode (4.1 eV). The relative yields for the two data sets are not to scale, but have been normalized to aid comparison. The dashed baselines have also been shifted up from zero for display purposes. The E_{trans} "window" of 0.13–0.20 eV is obtained by increasing the electron-pulse width to 1.0 μs and setting the laser delay time to 5.5 μs. To obtain the actual yield of $NO(\nu=0)$ as a function of these energies, one can use the yield at 100 eV from Fig. 9.
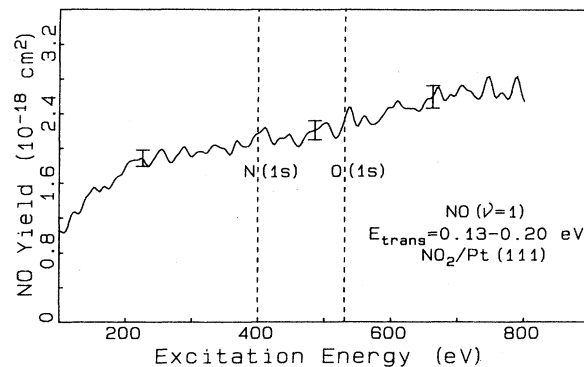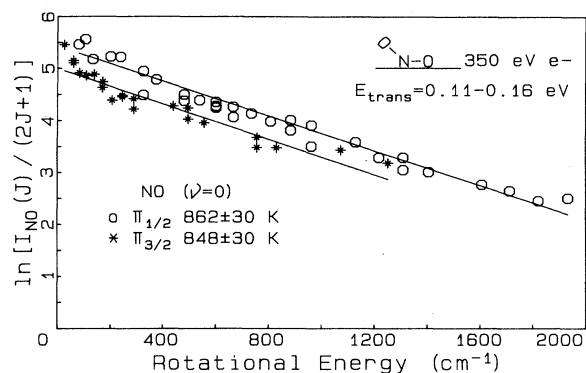
FIG. 10. Rotational-energy distribution for the NO($v=0$) product of NO_2 (0.5 ML) dissociation on Pt(111). The $^2\Pi_{1/2}$ data are obtained from the $P_{21}Q_{11}$ and $R_{11}Q_{21}$ bands, and the $^2\Pi_{3/2}$ data are obtained from the $P_{22}Q_{12}$ and $R_{12}Q_{22}$ bands of the $A^2\Sigma^+(0)\leftarrow X^2\Pi_{3/2,1/2}(0)$ transition. The average rotational energies shown for the two spin-orbit levels are calculated from the slopes of the respective least-squares fit lines shown. The E_{trans} "window" of 0.11–0.16 eV is due to an electron-pulse width of 1.0 μs and a laser delay time of 6.0 μs.

FIG. 11. Rotational difference spectrum between the high E_{trans} (0.32±0.1 eV) and low E_{trans} (0.13±0.03 eV) channels shown in Fig. 6. Two separate spectra are obtained at the corresponding delay times; the computer alternates between the delay times as the dye laser is scanned. The data are normalized at $R_{11}Q_{21}$ ($J=16.5$) to account for the energy spreads before the difference is computed. The three main rotational bands are shown, with J increasing to the right. A clear enhancement in high rotational levels is seen for the high-E_{trans} channel.

ponents.) Similar results are found for the $v=1$ and 2 levels. A summary of the observed internal state distributions is given in Table I.

Since the data in Fig. 10 are normalized with the degeneracy factor $2J+1$, it is assumed that the rotational angular momentum is spatially isotropic in the laser beam. For high-J levels the alignment of the angular momentum may, in fact, be parallel or perpendicular to the laser polarization, in which case rotation of the laser polarization will change the signal intensity.[29] To check for alignment, a double Fresnel rhomb was used to rotate the laser polarization 90° while the $P_{21}Q_{22}$ ($J=\frac{59}{2}$) signal signal was monitored. No changes were observed, even at the greatly reduced laser intensities used to minimize saturation effects.[29] Thus there is no significant molecular alignment in the laser beam. The NO may still leave the surface rotating in a specific plane with respect to the surface, but this information appears to be lost en route to the laser beam.[7] In a similar vein, there is no evidence for a $\Lambda(A')$ or $\Lambda(A'')$ (Ref. 43) propensity, as was seen for the ESD of NO.[7]

The vibrational population distribution is determined by two methods. The first method is to integrate over each rotational spectrum (raw data) from the $P_{21}Q_{11}$ bandhead to be R_{21} ($J=\frac{41}{5}$) line. The second method is to use the near-statistical fit of the rotational distributions and sum over calculated line intensities. Although both methods had very close agreement, the latter method may be more accurate in that it utilizes individually resolved rotational lines which are free from possible contributions from the high-J levels of the $^2\Pi_{3/2}$ state. The data are then normalized with the proper Franck-Condon factors[44] for the $A^2\Sigma^+(v')\leftarrow X^2\Pi_{1/2}(v'')$ transition.

Transitions probing higher-lying vibrational populations (v'') were attempted: $(v',v'')=(2,8)$ at 289 nm;

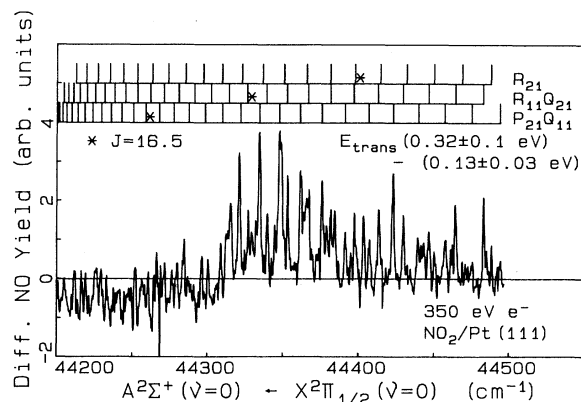$(v',v'')=(1,6)$ at 280 nm, $(v',v'')=(0,5)$ at 285 nm, and $(v',v'')=(3,3)$ at 220 nm. So far, no detectable population has been observed for any of these levels; however, the Franck-Condon factors for some of these transitions are relatively small.[44] From these results it appears that vibrational excitation in the NO dissociation product is considerably less than that observed in the gas phase (Sec. II).

The $v=0$ population of the NO $^2\Pi_{1/2}$ spin-orbit ground state was found to be a factor of 1.5 greater than that of the upper (by 121 cm^{-1}) $^2\Pi_{3/2}$ state. Although this ratio was not determined for the $v=1$ and 2 levels due to spectral overlap in the $^2\Pi_{3/2}$ band, no significant departure from the $v=0$ result is apparent. In the gas-phase 337-nm photodissociation of NO_2, the NO product has been observed also to have a $^2\Pi_{1/2}$ population about 1.5 times $^2\Pi_{3/2}$; this ratio was found to increase with increasing vibrational energy.[15] In the case of two-photon 450-nm photodissociation,[45] $^2\Pi_{1/2}\approx{}^2\Pi_{3/2}$ for $v=0$.

TABLE I. Energies of NO product from NO_2Pt(111) dissociation.

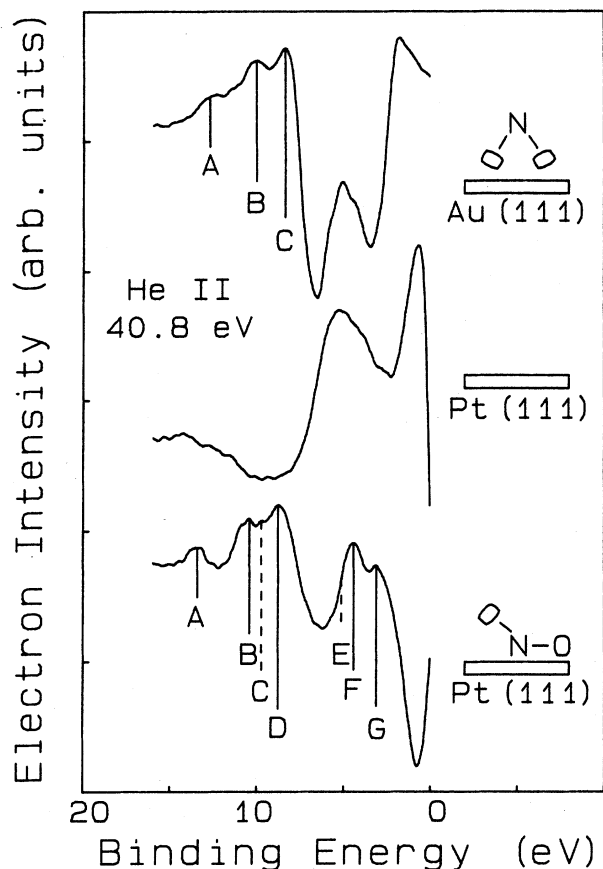| v	Population[a]	E_{trans} peak (eV)	E_{rot} (K)
0	NO "bulb"		299±4
0	1.00	0.15	862±30
0	0.67 ($^2\Pi_{3/2}$)	0.15	848±30
1	0.96±0.01	0.20	821±35
2	0.52±0.13	0.20	743±29

[a]Relative to $^2\Pi_{1/2}(v=0)$.

FIG. 12. He II (40.8 eV) ultraviolet photoelectron spectra (UPS) for NO₂ adsorbed on Au(111) (top) and Pt(111) (bottom). The UPS data for clean Pt(111) are shown in the middle. All the data were obtained from Bartram and Koel (Ref. 10). The assignments, which are discussed in the text and presented in Table II, were made in part on the basis of gas-phase UPS data published by Brundle et al. (Ref. 46). The dotted lines are for estimated line positions that are not fully resolved.

V. DISCUSSION

A. Electronic excitation: Structure and lifetimes

A comparison of data for electron-stimulated dissociation of adsorbed NO₂ with that of gas-phase photodissociation reveals some major differences. In the present work the threshold for dissociation is > 10 eV, far above the gas-phase dissociation energy of 3.1 eV. As discussed below, the shallow low-energy excitations which are very dissociative in the gas phase are ineffective on the surface because of their extremely short lifetimes in the presence of degenerate metal levels. The considerable reduction in internal excitation, particularly vibrational, relative to the gas-phase results (Sec. II) raises some important questions concerning the nature of the forces in the excited state.

Much of the discussion in this section will be concerned with bonding, excited-state thresholds, and screening. We will show in the course of this discussion that the ideas are supported by UPS data from clean Pt(111), NO₂ adsorbed on Pt(111), and NO₂ adsorbed on Au(111) recently acquired by Bartram, et al.[10] and shown in Fig. 12. The assignments for the UPS peaks are given in Table II and will be discussed at length near the end of this section. We begin our discussion of electronic structure by reviewing the detailed gas-phase results of Brundle et al.[46] The vertical ionization potentials of NO₂ and their state assignments from Ref. 46 are shown in Table II. Also listed is the primary molecular orbital (MO) involved in each excitation. These MO's fall into three families: the $3b_2$ and $4a_1$ principally involve p_σ oxygen orbitals which point roughly along the NO bond axes, the $1a_2$ and $1b_1$ orbitals involve $p_\perp$ orbitals which point out of the plane of the molecule, and the $6a_1$, $4b_2$, and $5a_1$ orbitals involve $p_\parallel$ orbitals which are within the molecular plane and roughly perpendicular to the NO bonds. The shallowest orbital, the $6a_1$, interacts most strongly with the substrate not only because of its low en-

TABLE II. The gas-phase vertical ionization potentials and assignments from Brundle et al. (Ref. 46) are compared with the NO₂/Pt(111) UPS results of Bartram et al. (Ref. 10) as seen in the bottom spectrum of Fig. 12, where the peaks are labeled from A to G. The shifts from gas to adsorbed phase are also shown. The atomic-orbital (AO) "family" of the molecular orbital is indicated. (NA denotes not applicable.)

State (orbital)	AO family	Gas phase (eV)	Adsorbed (eV)	Shift (eV)	Fig. 12
$^1A_1\ (6a_1)^{-1}$	$p_\parallel$	11.2	3.1	N/A	G
$^3B_2\ (4b_2)^{-1}$	$p_\parallel$	13.0	4.4	8.6[b]	F
$^3A_2(1a_2)^{-1}$	$p_\perp$	13.6	5.0[a]	8.6[a]	E
$^3A_1\ (5a_1)^{-1}$	$p_\parallel$	17.6	8.7	8.9[b]	D
$^3B_1\ (1b_1)^{-1}$	$p_\perp$	17.5	9.8[a]	7.7[a]	C
$^3B_2\ (3b_2)^{-1}$	p_σ	18.9	10.5	8.4	B
$^3A_1\ (4a_1)^{-1}$	p_σ	21.3	13.4	7.9	A

[a]Not resolved, only estimated.

[b]The shifts of these levels are reduced by hybridization of the $6a_1$ level with the substrate by about 0.3–0.6 eV. Of course, the shift of the $6a_1$ level is interpreted differently since it has been rehybridized with the substrate (see text).

ergy and partial occupancy (one electron), but also because the $p_\parallel$ lobes have the strongest (i.e., σ-like) interactions with the substrate orbitals in the geometry of NO_2 chemisorbed on Pt(111).

We need to discuss several effects in order to understand the lifetimes of shallow excitations in the chemisorbed species. If the adsorbate single-hole excitation is degenerate with substrate valence levels, the hole can be filled by direct resonant tunneling. The tunneling rate is determined by the transfer integral between adsorbate and substrate levels. In a small molecule such as NO_2, every orbital has appreciable contact with the substrate, so we would expect transfer integrals to be large (>0.1 eV) for all energetically allowed resonant decay channels. The resulting excitation lifetimes of $<10^{-15}$ s are too short to allow atomic motion for dissociation. Since the valence band of Pt(111) extends to 7 eV below the Fermi level E_F (see middle of Fig. 12), we can therefore exclude on the basis of short lifetimes all excitations within 7 eV of E_F. Excitations which are deeper than 7 eV below E_F decay predominantly via Auger processes involving electrons in the shallower molecular levels.

In forming the chemisorption bond, the normally half-filled $6a_1$ orbital mixes with substrate orbitals forming bonding ($6a_{1B}$) and antibonding ($6a_{1A}$) combinations, the former being filled with two electrons and the latter being empty [a situation analogous to the 2π bonding and antibonding orbitals of chemisorbed NO (Ref. 47)]. In the photoemission final state, the $6a_{1B}$ orbital rehybridizes because the $6a_1$ MO component is drawn down in energy by the presence of positively charged valence holes in the molecule. This rehybridization transfers charge onto the molecule, increasing the weight of the $6a_1^2$ configuration up from the $\frac{1}{4}$ neutral ground-state probability. Two electrons in the $6a_1$ MO are thus more readily available for the Auger decay of a valence hole in deeper orbitals. The presence of the "screening electron" in the antibonding $6a_1$ MO disrupts the NO_2 molecule as occurs in the gas-phase $^2B_2$ states. Unlike the gas phase, however, the $6a_{1B}$ electrons are shared with the metal so that the weight of the $6a_1^2$ configuration is appreciably less than unity even with the presence of two valence holes.

The first major point is that, even though we may make valence holes in such nonbonding orbitals as the $3b_2$,[46] the chemisorbed molecule falls apart not due to the primary hole, but due to the transfer of screening charge into the $6a_1$ strongly antibonding MO by rehybridization of the $6a_{1B}$ orbital. This charge transfer is present for all valence excitations. For example, the $3b_2$ ionization in the chemisorbed species is really more like a $3b_2^{-1}6a_1^{+\zeta}$ excitation, where $0<\zeta<1$.

The second major point is that, as shown by our previous work,[8] the longest-lived shallow valence excitations are those which are the highest in each MO "family" ($p_\parallel, p_\sigma, p_\perp$). If not degenerate with substrate bands, holes in the highest orbitals of each family Auger decay via electrons from different atomic orbitals (AO's). This introduces a factor of $1/(2l+1)^2$ in the Auger decay rate, where l is the angular momentum which must be transferred. Applying this simple rule to NO_2, we im-

mediately find that since the screening charge is in the $p_\parallel$ family of orbitals (so that any decay in this family can use the $6a_1^2$ configuration and proceed rapidly), the longest-lived single hole will be the $3b_2$ from the p_σ family. Normally, a $1a_2$ hole from the $p_\perp$ family would also be long lived; however, since the latter is degenerate with the substrate d bands (see Fig. 12), it need not decay via an Auger process, but can decay much faster by resonant tunneling. Since its lifetime is an order of magnitude or more longer than any other, we conclude that there is only one "long-lived" single-hole excitation, the $3b_2^{-1}6a_1^{+\zeta}$, which will dominate single-hole dissociation.

Two-hole excitations also contribute to stimulated desorption and dissociation.[41] Both single- and two-hole channels were observed[1,8] in the ESD of NO. In the present case we expect the $1a_2^{-2}$ excitation to be the longest-lived two-hole state because the $p_\perp$ orbitals are truly perpendicular to the $p_\parallel$ orbitals (which make up the higher levels used in Auger decay), while the p_σ orbitals of the $3b_2$ orbital are only approximately perpendicular to the $p_\parallel$. Using the Mulliken populations from Ref. 46 and noting that to lowest order the lifetime is proportional to the product of the populations, we estimate that in the absence of resonant tunneling processes a $1a_2$ hole is approximately twice as long lived as a $3b_2$ hole. Resonant tunneling would be curtailed if the hole-hole interaction in the $1a_2^{-2}$ state breaks the degeneracy of the $1a_2$ hole with the substrate valence band. From Fig. 12 we see that the screened hole-hole interaction energy U equal to 2 eV is required to break the degeneracy. This value for U is reasonable since the two holes cannot be completely screened from each other if the $6a_1$ orbital can accept, at most, only one screening electron. In the case of CO,[48,49] where it is possible that the two holes can be fully screened, valence Auger spectra have revealed $U\approx 2$ eV.

The cross section for creating the two-hole excitation, via a shakeoff process, is less than that for single-hole excitations, typically by a factor of about $5-10$. The two-hole excitation can also be made by the Auger decay of deeper single-hole excitations. Even with a factor of 5 lower excitation cross section, the longer lifetime of the two-hole state and the larger forces in the excited state make it plausible that the yield from the $1a_2^{-2}$ is comparable to that from the $3b_2^{-1}$ state. Thus we propose that these two excitations, both screened by charge in the $6a_1$ level, are the most probable channels observed in the experiment (Sec. V B). From the UPS data of NO_2 adsorbed on Pt(111), we see in Fig. 12 that the assignment of the $3b_2^{-1}$ and $1a_2^{-2}$ excited states do correspond to the 10–15-eV dissociation threshold observed in the experiment.

From Table II we see that the shift in photoelectron energy between adsorbed and gas-phase NO_2 is $\sim 8-9$ eV $=\phi_{Pt}$ (5.8 eV)$+\Delta E_S$(2–3 eV), where the ΔE_S term, which includes chemical (i.e., rehybridization) effects and screening shifts for the excitations, is consistent with values reported by Brundle.[50] Three effects are of relevance here. First, the shift between the gas-phase and chemisorbed systems of the two orbitals in the p_σ family

(the $4a_1$ and $3b_2$) are slightly different. We see that the shifts are the same, however, in the $NO_2/Au(111)$ system, where the molecule has a O,O-nitrito bonding geometry which preserves the equivalence of the oxygen sites[51] (see peaks A and B in the top spectrum of Fig. 12). Because the shift difference for the $NO_2/Pt(111)$ system is small compared with the energy difference of the MO's, we conclude that there is only slight rehybridization due to oxygen-site inequivalency, so that the rehybridization is not sufficient to warrant abandonment of the MO labels. Second, we note a slightly greater shift for the MO levels in the $p_\parallel$ family than for others. We interpret this as being due to better screening since these holes occupy the same AO type as the screening charge. Third, within the one-electron tight-binding approximation, we can model the effects of chemisorption on the $p_\parallel$ family by diagonalizing the following Hamiltonian matrix:

$$\begin{bmatrix} \partial & -\gamma & 0 & 0 \\ -\gamma & \partial & -\gamma & -\delta \\ 0 & -\gamma & \partial & \delta \\ 0 & -\delta & \delta & \beta \end{bmatrix},$$

where ∂ is the energy of the three $p_\parallel$ orbitals which compose the three MO's in the gas phase (taken to be the same), γ is the π-like transfer matrix elements between the orbitals within the molecule, β is the energy of the Pt d level(s) which bond to the molecule, and δ is the interaction between the two $p_\parallel$ AO's of the molecule and the metal level. We set γ by the energy splitting of the $5a_1, 4b_2$, and $6a_1$ levels in the gas phase, ∂ by the approximate position of the (chemisorbed) orbitals with respect to E_F, β close to E_F (-1 eV), and δ by the need to place the $6a_{1B}$ level at -3.1 eV. (Inverse photoemission could locate the position of the empty $6a_{1A}$ orbital; without this information, the model parameters are somewhat arbitrary.)

Although we have used a simple model, we are able to make the following general conclusions. (1) δ must be quite large; otherwise the gas-phase splitting of the $p_\parallel$ orbitals places the $6a_1$ too close to E_F, given the position of the other two. The large δ causes the $6a_{1B}$ to be roughly a 50-50 mixture of metal and $6a_1$ character, thus causing the molecule to be essentially neutral in its chemisorbed ground state. However, a large δ also causes the excited-state screening to be "incomplete" because the $6a_{1B}$ excited-state orbital would retain appreciable metal character. (2) For any reasonable choice of δ, bonding to the surface causes only slight rehybridization of the lower two $P_\parallel$ orbitals, causing a shift *away* from E_F of <0.5 eV. This supports our argument discussed above for the cause of the greater shift in this family of orbitals being due to better screening.

The "long-lived" excitations, one hole in the $3b_2$ or two holes in the $1a_2$ orbitals, are very rapidly (10^{-16} s) screened by the metal through the $6a_1$ orbital. Since the $3b_2$ and $1a_2$ orbitals are shown by gas-phase photoemission to be nonbonding in character,[46] the presence of one or two holes in either orbital should not significantly change the NO bond lengths or ONO bond angle. How-

ever, the presence of screening charge in the $6a_1$ orbital will weaken the NO bonds and decrease the ONO bond angle, so that the NO_2 may electronically approach O_3, where $\alpha = 116.8°$, $r_0 = 1.28$ Å, and the dissociation energy has been reduced to 1.0 eV.[16]

B. Dissociation dynamics

In the gas-phase dissociation of NO_2, most of the excess electronic excitation energy is found in the ground-state NO and $O(^3P)$ products. Although translational energies of the latter are not well characterized for excitation energies much above the dissociation threshold, a considerable portion of the excess energy is found in vibrational and rotational excitation of the NO. As discussed in Sec. II, the extensive excitation of internal energies is associated with Franck-Condon transitions to high ro-vibronic levels associated with excited states having large ONO bond-angle and NO bond-length changes relative to the ground state. In contrast to the gas-phase dissociation of NO_2, the translational and internal energies of the dissociated NO leaving the surface are an insignificant fraction of the excess excitation energy because the electronic energy is rapidly quenched by the substrate. However, the presence of screening charge in the $6a_1$ should still induce large geometry changes.

If the screened excitations of NO_2 on the Pt surface electronically approach the geometry of O_3 in that there is extra charge density in the $6a_1$ orbital, then the NO (or "O_2") bond length in this state would be close to $r_0 = 1.28$ Å, which is significantly longer than the NO gas-phase value of $r_0 = 1.15$ Å. In gas-phase dissociation, such Franck-Condon transitions result in considerable vibrational excitation. For example, in the 248.5-nm photodissociation of NO_2 through the $\tilde{B}\,^2B_2$ state, where $r_0 = 1.31$ Å, the vibrational distribution peaks at $v = 7$ (Sec. II). Thus a large amount of vibrational excitation is expected in the NO product if nuclear motion occurs on an "O_3"-like electronically excited state of $NO_2/Pt(111)$. However, the vibrational distribution which is observed, $v = 0,1,2 = (1.0):(0.96):(0.52)$, is much lower in energy than is expected from the "O_3" state.

The rotational excitation is also less than expected in going from one electron in the $6a_1$ orbital to full occupancy. The reduced bond angle for the fully screened excited NO_2 (or "O_3") will move the noncoordinated NO bond closer to the surface normal and is expected to impart some angular momentum to the NO product. This effect is observed in the gas phase, where, if one again looks to the 248.5-nm photodissociation through the $\tilde{B}\,^2B_2$ state, where $\alpha = 121°$, the rotational excitation of the NO product is highly non-Boltzmann, with population in rotational levels approaching the thermodynamic limit for each vibrational level. For the case of NO_2 dissociation on the Pt surface, one sees a much lower rotational excitation in the NO product. In fact, the average rotational energy of $\sim 750–860$ K for all three observed vibrational levels is only 50% greater than the zero-point energy of 572 K of the NO_2 bend on Pt(111).[11] Thus most of the rotational energy is from ground-state zero-

point motion of the parent molecule. This is exactly what was observed in the ESD of NO, where the 335-K zero-point energy was derived from the hindered rotor of the NO—Pt bond.[6] In the latter, the 50% "rotational heating" was due to an increased probability for desorption with rotational energy.[7] In the present case the rotational heating may come from a similar consequence.

There are two possible reasons why one does not observe extensive vibrational and rotational excitation of the NO product as in the gas phase. Both arguments have the same effect and are not mutually exclusive. The first explanation is that screening via the antibonding $6a_1$ level is incomplete. Since bond-angle and bond-length changes are associated with charge density in the $6a_1$ orbital, partial screening will reduce these changes. The second explanation is that the ground-state geometry of NO_2 on Pt(111) *already resembles* O_3 by virtue of rehybridization caused by the metal through bonding with the $6a_1$; thus bond angles and bond lengths would be changed less upon excitation.

If the $3b_1^{-1}$ excitation is only partially screened by the metal-$6a_1$ charge (i.e., if the weight of the $6a_1^2$ configuration in the excited state is significantly less than unity due to the large value of the metal-to-$6a_1$ transfer integral δ), then much smaller changes in NO bond length and ONO bond angle are expected than if the full two-electron charge is present in the $6a_1$ as in the gas phase. Thus the extent of vibrational and rotational excitation would be dependent on the actual value of ζ in the $3b_2^{-1}6a_1^{+\zeta}$ electronic excitation. Evidence for this notion is found in the E_{trans} shifts to higher energy observed in Figs. 5 and 6 for increasing vibrational and rotational excitation. These shifts are most likely due to the differences in screening charge for the one-hole $3b_2^{-1}6a_1^{+\zeta}$ excitation and the two-hole $1a_2^{-2}6a_1^{+\zeta'}$ excitation. Since $\zeta' > \zeta$, the two-hole excitation results in more NO vibrational and rotational energy. The antibonding character of the $6a_1$ orbital is also evident in the slight increase in E_{trans} associated with the two-hole excitation. More dramatic shifts in E_{trans} with vibration have been seen for the ESD of NO,[1,6] due to the variation in charge density in the 2π orbital, but it is significant that no shifts in the NO ESD E_{trans} are observed versus rotational energy since there is no mechanism for rotational excitation in the NO excited state (i.e., bond-angle changes) other than release of the zero-point energy of the hindered rotor.[7]

Support for the second explanation comes from the vibrational spectra of ground-state NO_2 on Pt(111) discussed by Bartram, Windham, and Koel.[11] They found that shifts in the stretching frequencies resembled those observed for equivalently bonded (NO bridge-bonded nitrito) cobalt and platinum NO_2 complexes. The shifts are due to an inequality of the NO bond lengths: in the cobalt complex $[Co(NH_3)_3(OH)(NO_2)_2Co(NH_3)_3]^{3+}$, the coordinated NO bond length is 1.29 Å, whereas the noncoordinated bond length is 1.21 Å.[52] Thus not only do the NO bond lengths for the cobalt-NO_2 complex bracket those of O_3, but the noncoordinated bond length is closer to that of gaseous NO. Metallic screening in the excited

state would be expected to further reduce the noncoordinated NO bond length (making it closer to gaseous NO) while increasing the coordinated bond length. The ONO bond angle for the cobalt complex is 115°,[10] which is very close to the O_3 angle of 116.8°. Thus only a small change in bond angle upon electronic excitation is not unrealistic. The observed rotational-energy distributions can now be explained adequately by the zero-point energy of the ground-state bending motion. The 50% "rotational heating" above the zero point cannot be understood in the absence of quantum-dynamics calculations, especially since the cause of the effect may be due to the ground state (as in NO ESD) or the excited-state potential-energy surfaces, or both.

Undoubtedly, the observed translational and internal energies of the NO product are due to some combination of both factors discussed above. Comparison of the NO translational energy distributions with those found in gas-phase dissociation are inconclusive due to the scarcity of gas-phase data. However, the observed range 0.1–0.6 eV (including the high-energy tail) is similar to the total energy of *both* fragments reported by Busch and Wilson[13] (see Sec. II).

VI. SUMMARY AND CONCLUSIONS

We have found that the electron-stimulated dissociation of NO_2 on Pt(111) is brought about by the creation of excitations that are much more energetic than those required for gas-phase dissociation. We believe that the low-energy excitations (3–5 eV) which are analogous to those giving rise to gas-phase dissociation have lifetimes that are much too short to allow dissociation on the surface because they are resonant with the metal valence density of states. Excitations that dominate adsorbate dissociation do so because of longer lifetimes. For nonresonant excitations, those having the longest lifetimes have different atomic-orbital makeup relative to higher (shallower) orbitals, so that Auger decay must involve a change in electronic angular momentum. Lifetime considerations indicate that the 10–15-eV threshold is associated with two excitations: the one-hole $3b_2^{-1}6a_1^{+\zeta}$ excitation and the two-hole $1a_2^{-2}6a_1^{+\zeta'}$ excitation, where $\zeta' > \zeta$ represents the net effect of screening through the $6a_1$-metal interaction.

The dynamics of the dissociation process thus progresses with increasing charge-transfer screening in the $6a_1$ level from the ground-state geometry to the geometry associated with the O_3 molecule and the electronically excited gas-phase NO_2: a smaller ONO bond angle and longer, weaker NO bonds. However, there is much less vibrational and rotational excitation in the NO product than observed in gas-phase photodissociation. Thus the weight of the $6a_1^2$ configuration in the excited state must be significantly less than unity. This conclusion is supported by the analysis of photoemission spectra where a large interaction between the metal and the $6a_1$ MO is deduced. The effects of increased screening associated with the two-hole excitation are observed in the form of shifts in the translational energy distribu-

tions for vibrationally and rotationally hot NO products. Another important factor for the lack of internal excitation in the NO product may be that the ground-state geometry itself resembles O$_3$, due to the effects of bonding to the metal substrate. Thus, geometry changes due to screening may be minimized. In conclusion, the presence of screening on the metal surface has profound effects on the stimulated dissociation of adsorbed molecules. In the present case, not only are the lifetimes of excitation channels limited by screening, but also the dynamics of the

dissociation are a direct function of charge transfer from the metal.

[1]A. R. Burns, E. B. Stechel, and D. R. Jennison, in *Desorption Induced by Electronic Transitions, DIET III*, edited by R. H. Stulen and M. L. Knotek (Springer-Verlag, New York, 1988), pp. 67–72.

[2]E. P. Marsh, M. R. Schneider, T. L. Gilton, F. L. Tabares, W. Meier, and J. P. Cowin, Phys. Rev. Lett. **60**, 2551 (1988).

[3]D. Coulman, A. Pushmann, W. Wurth, H.-P. Steinrück, and D. Menzel, Chem. Phys. Lett. **148**, 371 (1988).

[4]D. E. Ramaker, J. Chem. Phys. **78**, 2998 (1983); Chem. Phys. **80**, 183 (1983).

[5]P. Avouris and B. N. J. Persson, J. Phys. Chem. **88**, 837 (1984).

[6]A. R. Burns, E. B. Stechel, and D. R. Jennison, Phys. Rev. Lett. **58**, 250 (1987).

[7]A. R. Burns, E. B. Stechel, and D. R. Jennison, J. Vac. Sci. Technol. A **6**, 895 (1988).

[8]D. R. Jennison, E. B. Stechel, and A. R. Burns, in Ref. 1, pp. 167–172.

[9]E. B. Stechel, D. R. Jennison, and A. R. Burns, in Ref. 1, pp. 136–143.

[10]M. E. Bartram and B. E. Koel (unpublished).

[11]M. E. Bartram, R. G. Windham, and B. E. Koel, Surf. Sci. **184**, 57 (1987).

[12]I. T. Jones and K. D. Bayes, J. Chem. Phys. **59**, 4836 (1973).

[13]G. E. Busch and K. R. Wilson, J. Chem. Phys. **56**, 3626 (1972).

[14]M. Mons and I. Dimicoli, Chem. Phys. Lett. **131**, 298 (1986).

[15]H. Zacharias, M. Geilhaupt, K. Meier, and K. H. Welge, J. Chem. Phys. **74**, 218 (1981).

[16]G. Herzberg, *Electronic Spectra of Polyatomic Molecules* (Van Nostrand/Reinhold, New York, 1966), pp. 602–604.

[17]C. G. Stevens and R. N. Zare, J. Mol. Spectrosc. **56**, 167 (1975).

[18]T. G. Slanger, W. K. Bischel, and M. J. Dyer, J. Chem. Phys. **79**, 2231 (1983).

[19]K.-E. J. Hallin and A. J. Merer, Can. J. Phys. **54**, 1157 (1976).

[20]R. J. S. Morrison, B. H. Rockney, and E. R. Grant, J. Chem. Phys. **75**, 2643 (1981).

[21]L. Bigio and E. R. Grant, J. Chem. Phys. **87**, 360 (1987).

[22]M.-R. Taherian, P. C. Crosby, and T. G. Slanger, J. Phys. Chem. **91**, 2304 (1987).

[23]R. K. Ritchie and A. D. Walsh, Proc. R. Soc. London, Ser. A **267**, 395 (1962).

[24]A. R. Burns, D. R. Jennison, and E. B. Stechel, J. Vac. Sci. Technol. A **5**, 671 (1987).

[25]Cut and polished by Metal Crystals + Oxides, Ltd., Cambridge, England.

[26]J. L. Gland, B. A. Sexton, and G. B. Fischer, Surf. Sci. **95**, 587 (1980).

[27]D. Dahlgreen and J. C. Hemminger, Surf. Sci. **123**, L739 (1982).

[28]Gerhard Herzberg, *Spectra of Diatomic Molecules* 2nd ed. (Van Nostrand/Reinhold, New York, 1950), pp. 264 and 558.

[29]D. C. Jacobs, R. J. Madix, and R. N. Zare, J. Chem. Phys. **85**, 5469 (1986).

[30]Lester T. Earls, Phys. Rev. **48**, 423 (1935).

[31]R. Engleman, P. E. Rouse, H. M. Peek, and V. D. Biamonte, Los Alamos Scientific Laboratory Report No. LA-4364, 1970 (unpublished).

[32]K. P. Huber and G. Herzberg, *Molecular Spectra and Molecular Structure, Constants of Diatomic Molecules* (van Nostrand/Reinhold, New York, 1979), Vol. IV.

[33]J. L. Gland, Surf. Sci. **71**, 327 (1978).

[34]D. J. Bamford, L. E. Jusinski, and W. K. Bischel, Phys. Rev. A **34**, 185 (1986).

[35]B. H. Rockney, G. E. Hall, and E. R. Grant, J. Chem. Phys. **78**, 7124 (1983).

[36]T. E. Madey and J. T. Yates, Jr., J. Vac. Sci. Technol. **8**, 525 (1971).

[37]D. Menzel, in *Interactions on Metal Surfaces, Topics in Applied Physics*, edited by R. Gomer (Springer-Verlag, New York, 1975), Vol. 4, p. 128.

[38]K. Stephan, H. Helm, Y. B. Kim, G. Seykora, J. Ramler, M. Grossl, E. Märk, and T. D. Märk, J. Chem. Phys. **73**, 303 (1980).

[39]M. E. Bartram, R. G. Windham, and B. E. Koel, Langmuir **4**, 240 (1988).

[40]M. E. Bartram, B. E. Koel, and E. A. Carter, Surf. Sci. **219**, 467 (1989).

[41]R. Jaeger, R. Treichler, and J. Stohr, Surf. Sci. **117**, 533 (1982).

[42]R. Treichler, W. Riedl, W. Wurth, P. Feulner, and D. Menzel, Phys. Rev. Lett. **54**, 462 (1985).

[43]M. H. Alexander *et al.*, J. Chem. Phys. **89**, 149 (1988).

[44]*Spectroscopic Data*, edited by S. N. Suchard (IFI/Plenum, New York, 1975), Vol. 1, pp. 308–347 (CO) and pp. 720–743 (NO).

[45]R. J. S. Morrison and E. R. Grant, J. Chem. Phys. **77**, 5994 (1982).

[46]C. R. Brundle, D. Neumann, W. C. Price, D. Evans, A. W. Potts, and D. G. Streets, J. Chem. Phys. **53**, 705 (1970).

[47]S. Ferrer, K. H. Frank, and B. Reihl, Surf. Sci. **162**, 264 (1985).

[48]B. E. Koel, J. M. White, and G. M. Loubriel, J. Chem. Phys. **77**, 2665 (1982).

[49]E. Umbach and Z. Hussain, Phys. Rev. Lett. **52**, 257 (1984).

[50]C. R. Brundle, J. Vac. Sci. Technol. **13**, 301 (1976).

[51]M. E. Bartram and B. E. Koel, Surf. Sci. **213**, 137 (1989).

[52]M. A. Hitchman and G. L. Rowbottom, Coord. Chem. Rev. **42**, 55 (1982).